INTRODUCTION TO GENERALIZED PARTON DISTRIBUTIONS

M. Diehl
Institut für Theoretische Physik E, RWTH Aachen, 52056 Aachen, Germany

Abstract
I give a brief introduction to generalized parton distributions, their physics, and opportunities for measuring them in μp collisions.

1. WHAT ARE GENERALIZED PARTON DISTRIBUTIONS?

Generalized parton distributions (GPDs) [1–4] have been recognized in the last few years as a tool to study hadron structure in new ways. Unifying the concepts of parton distributions and of hadronic form factors, GPDs contain a wealth of information about how quarks and gluons make up hadrons. Advances in experimental technology raise the hope of studying the exclusive processes where these functions appear.

The study of ordinary parton distributions provides us with detailed knowledge about the distribution of momentum and spin of quarks, antiquarks, and gluons. It is, however, important that the momentum probed in this way is the *longitudinal* momentum of the partons in a fast moving hadron. All information about the *transverse* structure is integrated over in the parton densities. One has in particular lost information about the role of the orbital angular momentum of partons in making a proton of total spin $\frac{1}{2}$. Clearly, orbital angular momentum should play a role at resolution scales where one can talk about partons: the simple splitting process $q \to qg$ of a light quark moving along the z-axis generates orbital angular momentum L_z, since this is the only way for it to conserve the total angular momentum J_z [5]. In order to access such information one needs quantities that involve transverse momenta, and this can be achieved in the exclusive scattering processes described by GPDs.

A good example to see the similarities and differences between usual parton densities and their generalization is the Compton amplitude. Via the optical theorem, the cross section for inclusive deep inelastic scattering (DIS) can be obtained from the imaginary part of the *forward* amplitude $\gamma^* p \to \gamma^* p$. In the Bjorken region of large photon virtuality Q^2 and collision energy, this amplitude factorizes into a parton distribution and a perturbatively calculable scattering process at the level of quarks and gluons. The simplest diagram for this is shown in Fig. 1a. The amplitude for deeply virtual Compton scattering (DVCS) $\gamma^* p \to \gamma p$, a completely exclusive process, factorizes in an analogous way if in addition to the Bjorken limit we require a small invariant momentum transfer t to the proton. Since the two proton momenta in the diagram of Fig. 1a are now different, the non-perturbative dynamics is not described by ordinary parton distributions, but by quantities which generalize them. In addition, the finite momentum transfer to the proton makes a second space–time structure of the process possible. Whereas in Fig. 1a the partonic subprocess is the scattering of a photon on a quark or antiquark, the virtual photon can also annihilate a quark–antiquark pair with transverse separation of order $1/Q$ in the proton target, as shown in Fig. 1b.

Like the usual parton densities, GPDs are defined through matrix elements of quark and gluon operators, for instance

$$\begin{aligned}(Pn) \int \frac{d\lambda}{2\pi}\, e^{i\lambda x (Pn)} \langle p', s' |\, \bar{q}(-\tfrac{1}{2}\lambda n)\, (n\gamma)\, q(\tfrac{1}{2}\lambda n)\, | p, s \rangle \\ = \quad \bar{u}(p', s')(n\gamma) u(p, s)\, H(x, \xi, t) + \bar{u}(p', s') \frac{i\sigma^{\alpha\beta} n_\alpha (p' - p)_\beta}{2m} u(p, s)\, E(x, \xi, t)\,. \end{aligned} \tag{1}$$

Here n is a light-like vector which determines the direction we call 'longitudinal'. These definitions provide the basis for deriving important properties of the distributions:

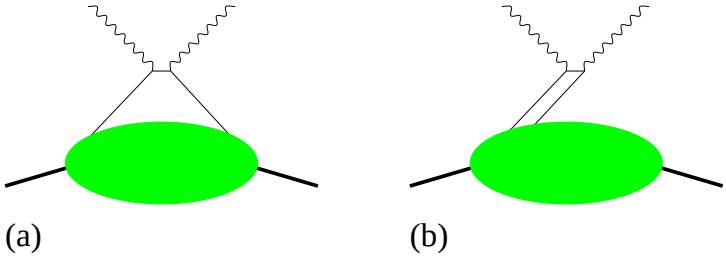

Fig. 1: Feynman diagrams for the Compton amplitude in the regime where it factorizes into a parton distribution and a hard partonic subprocess: (a) quark–photon scattering, (b) annihilation of a quark–antiquark pair.

- In the limit where the two states $|p, s\rangle$ and $p', s'\rangle$ become equal, one finds that H becomes the usual quark density, which thus provides boundary values for this function. On the other hand, the forward limit of the distribution E cannot be measured in the same way as usual parton distributions, since it appears multiplied by the momentum transfer $p' - p$. Evaluating the spinors in the right-hand side of Eq. (1) one finds in fact that E appears in the transition between a left- and a right-handed proton. Since the quark helicity remains the same, angular momentum balance requires orbital angular momentum, which is provided only if the proton momenta p and p' differ in their transverse components.
- Taking moments of these distributions in the momentum fraction x gives the matrix elements of *local* currents, for instance of the vector current in Eq. (1). The moments of GPDs are thus given by elastic form factors. The well-known electromagnetic Dirac and Pauli form factors, $F_1(t)$ and $F_2(t)$, are respectively obtained as lowest x-moments of the GPDs H and E. Of particular interest is the second moment $\frac{1}{2} \int dx\, x(H + E)$, whose value at $t = 0$ gives the *total* angular momentum of the quark species in question, including its spin and orbital angular momentum [2]. Note also that such moments are well suited to be calculated in lattice QCD.
- The quark–antiquark operator in Eq. (1) must be renormalized. The variation of the distributions with the renormalization scale μ is described by evolution equations that generalize the well-known DGLAP equations for parton densities, with evolution kernels known to two-loop accuracy [6]. Physically, μ^{-1} corresponds to the spatial resolution at which the partons are probed in the hard scattering process.

GPDs depend on three kinematical variables: x and ξ parametrize the independent longitudinal momentum fractions of the partons, whereas the dependence on $t = (p' - p)^2$ takes into account that there can also be a transverse momentum transfer. A very intuitive representation of the physics encoded in GPDs is obtained by a Fourier transform from $(p' - p)_\perp$ to transverse position $b_\perp$ [7–9]. The resulting picture is shown in Fig. 2. GPDs describe at the same time the longitudinal momentum of partons and their distance from the transverse 'centre' of the proton, and in this sense provide a fully three-dimensional

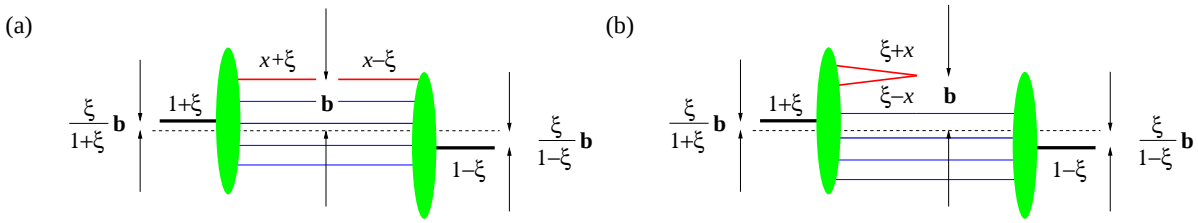

Fig. 2: Representation of a GPD in impact parameter space. Longitudinal momentum fractions refer to the average proton momentum $\frac{1}{2}(p + p')$ and are indicated above or below lines. The regions (a) and (b) correspond to those in Fig. 1.

image of partons in a hadron.

The usual parton densities are obtained in this picture by setting $\xi = 0$ and integrating over the transverse position $b_\perp$. Further analysis shows that the 'blobs' in Fig. 2 represent the light-cone wave functions of the incoming or the outgoing proton [10]. This highlights another difference between GPDs and their forward limit. Usual parton densities are given by squared wave functions and therefore represent probabilities. In contrast, GPDs correlate wave functions for different parton configurations and thus are genuinely quantum-mechanical interference terms. In region (b) they coherently probe $q\bar{q}$ pairs within the target.

There is an increasing amount of effort to better understand the dynamics of GPDs by various strategies of modelling them, a recent overview is given in Ref. [11]. Among many interesting features is the possibility to treat these quantities with methods of chiral perturbation theory and thus to investigate the role of chiral symmetry and its breaking in nucleon structure. Much remains to be done in this area: the rich physics content of GPDs is mirrored in a considerable complexity of their behaviour on x, ξ and t. Theoretical ideas will have to be tested against the constraints from data.

2. HOW TO MEASURE GENERALIZED PARTON DISTRIBUTIONS?

The appearance of GPDs in exclusive scattering processes is established by factorization theorems [12], which are very similar to those for inclusive processes such as DIS or Drell–Yan pair production. The foremost example is DVCS shown in Fig. 1. It is the process whose theory is most advanced, and the one which is probably the cleanest for extracting information on the unknown distributions. A large class of other reactions is provided by meson production, see Fig. 3. It provides a wealth of different channels and thus a handle to disentangle GPDs for different quark flavours and for gluons and to test the universality of the extracted functions. The comparatively large cross sections of some channels (for instance the production of ρ^0 mesons) will allow detailed studies in several kinematical variables. On the other hand the complexity of these processes, containing nonperturbative information on both the target and the produced meson, makes them more difficult to analyse. Also, there is reason to believe that the values of Q^2 where the simple factorized description of Fig. 3 is adequate, are larger than for DVCS, maybe 10 GeV^2 and more.

Fortunately there are predictions of factorization which can be tested directly in the data, without previous knowledge of the nonperturbative functions one aims to extract. In the limit of large Q^2 at fixed Bjorken variable x_B and fixed t, the amplitude for $\gamma^* p \to \gamma p$ should become independent of Q^2 up to logarithmic corrections; this is the precise analog of Bjorken scaling for DIS. The analogous scaling predicted for the meson production amplitude is like $1/Q$. In practice such tests require a sufficiently large lever arm in Q^2 at fixed x_B: for this the rather high beam energy of COMPASS presents an important advantage. A further prediction concerns the helicity structure of the process: at large Q^2 the dominant amplitudes for DVCS are for a transverse γ^*, whereas for meson production longitudinal γ^* and longitudinal meson polarization should dominate. Other polarizations are suppressed by further

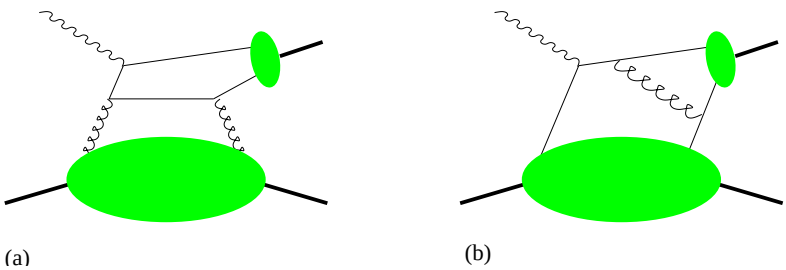

Fig. 3: Diagrams for meson leptoproduction with (a) gluon and (b) quark exchange with the target.

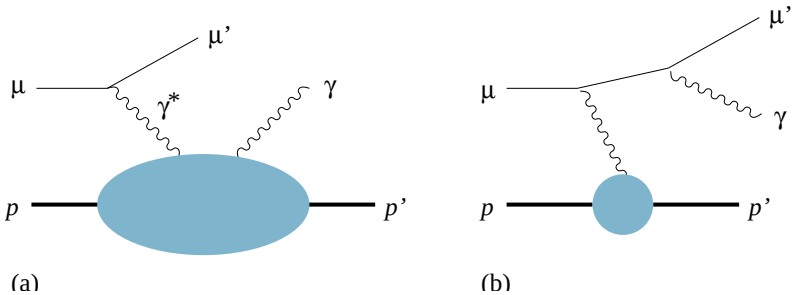

Fig. 4: Diagrams for the (a) Compton and (b) the Bethe–Heitler processes, contributing to leptoproduction $\mu p \to \mu p \gamma$.

powers of $1/Q$. The meson polarization is experimentally accessible from the decay angular distribution if the meson decays (for instance $\rho^0 \to \pi^+\pi^-$). Information on the polarization of the virtual photon is contained in the azimuthal angle φ between the hadron and the lepton planes in the leptoproduction process $\mu p \to \mu p \rho$, $\mu p \to \mu p \gamma$, etc. This angle corresponds in fact to a rotation around the momentum of the exchanged γ^* and is hence intricately related with the angular momentum along this direction.

The cleanest and most detailed access to the exclusive dynamics at amplitude level is possible in DVCS. In this case not only Compton scattering (Fig. 4a) but also the Bethe–Heitler process (Fig. 4b) contribute to the leptoproduction amplitude. Which mechanism dominates at given Q^2 and x_B depends mainly on the lepton beam energy E_ℓ. Large values of $1/y = 2m_p E_\ell \, x_B/Q^2$ favour DVCS and small values of $1/y$ favour Bethe–Heitler. The Bethe–Heitler process is completely calculable in QED, together with our knowledge of the elastic proton form factors at small t.

In kinematics where the Bethe–Heitler amplitude is sizeable, one can use the interference of the two processes to gain information about the Compton amplitude, including its phase. This is highly valuable since GPDs enter the $\gamma^* p$ amplitude through integrals of the type

$$\int dx \, \frac{H(x,\xi,t)}{x - \xi + i\epsilon}. \tag{2}$$

Since GPDs are real-valued due to time reversal invariance, the real and imaginary parts of this expression contain very distinct information on H. This information can be accessed in suitable observables, which can be identified by using the structure of the Bethe–Heitler and Compton processes at large Q^2 and small t, but without knowledge of the unknown Compton amplitudes [13]. To see how this works let us consider an unpolarized target and discuss the dependence of the cross section on the angle φ, and on the charge e_ℓ and longitudinal polarization P_ℓ of the muon beam. We schematically have

$$\begin{aligned}
&\frac{d\sigma(\mu p \to \mu p \gamma)}{d\varphi} \\
&= A_{\rm BH}(\cos(\varphi), \cos(2\varphi), \cos(3\varphi), \cos(4\varphi)) \\
&+ A_{\rm INT}(\cos(\varphi), \cos(2\varphi)) \Big(e_\ell \Big[c_1 \cos(\varphi) \, {\rm Re}\mathcal{A}(\gamma_T^*) + c_2 \cos(2\varphi) \, {\rm Re}\mathcal{A}(\gamma_L^*) + \ldots \Big] \\
&\qquad\qquad + e_\ell P_\ell \Big[s_1 \sin(\varphi) \, {\rm Im}\mathcal{A}(\gamma_T^*) + s_2 \sin(2\varphi) \, {\rm Im}\mathcal{A}(\gamma_L^*) \Big] \Big) \\
&+ A_{\rm VCS}(\cos(\varphi), \cos(2\varphi), P_\ell \sin(\varphi)),
\end{aligned} \tag{3}$$

where $A_{\rm BH}$, $A_{\rm INT}$, c_i, s_i are known expressions and $\mathcal{A}$ represents $\gamma^* p \to \gamma p$ amplitudes for different γ^* polarization. The $\ldots$ in brackets stand for a φ-independent term and a term with $\cos(3\varphi)$. Both are expected to be small in the kinematics under study but can readily be included in a full analysis. With muon beams one naturally reverses both charge and helicity at once, but we see how all four expressions in the interference can be separated: in the cross section difference $\sigma(\mu^+) - \sigma(\mu^-)$ the Bethe–Heitler

contribution $A_{\rm BH}$ drops out and one has access to the real parts of $\mathcal{A}(\gamma^*_{T,L})$. With angular analysis one can separate these two and test, for instance, the scaling predictions $\mathcal{A}(\gamma^*_T) \sim Q^0$ and $\mathcal{A}(\gamma^*_L) \sim Q^{-1}$ of the factorization theorem. In the sum of cross sections $\sigma(\mu^+) + \sigma(\mu^-)$ the imaginary parts of $\mathcal{A}(\gamma^*_{T,L})$ can be separated from the Bethe–Heitler and VCS contributions by their angular dependence, since their coefficients change sign under $\varphi \to -\varphi$ whereas the other contributions do not.

In the region of moderate to large x_B DVCS can be analysed along similar lines to meson production, if necessary after subtraction of the Bethe–Heitler term and integration over φ. Part of this kinematics overlaps with the x_B and Q^2 values where HERMES can access Compton amplitudes through the Bethe–Heitler interference due to its lower beam energy [14]. Comparison of data in this region will provide valuable cross checks, with the analysis in the interference region giving more detailed access to the Compton process and the analysis in the VCS dominated regime being less involved and hence more robust.

3. CONCLUSIONS

Generalized parton distributions permit one to study qualitatively new aspects of hadron structure, including detailed information on the longitudinal and transverse distribution of quarks and gluons, their orbital angular momentum, quantum mechanical interference effects, and $q\bar{q}$ pairs in the target wave function. The theory of how to measure these quantities in exclusive processes rests on solid foundations. Valuable data on Compton scattering and meson production can be obtained at COMPASS in a wide kinematical region, and with specific advantages from having polarized lepton beams of both charges.

Acknowledgements

I thank the organizers for their kind invitation to this workshop, and Nicole d'Hose and Dietrich von Harrach for valuable discussions.

References

[1] D. Müller, D. Robaschik, B. Geyer, F. M. Dittes, and J. Hořejši, Fortsch. Phys. **42** (1994) 101 [hep-ph/9812448].

[2] X. Ji, Phys. Rev. Lett. **78** (1997) 610 [hep-ph/9603249].

[3] A. V. Radyushkin, Phys. Rev. D **56** (1997) 5524 [hep-ph/9704207].

[4] J. Blümlein, B. Geyer, and D. Robaschik, Phys. Lett. B **406** (1997) 161 [hep-ph/9705264].

[5] P. G. Ratcliffe, Phys. Lett. B **192** (1987) 180.

[6] A. V. Belitsky, A. Freund, and D. Müller, Nucl. Phys. B **574** (2000) 347 [hep-ph/9912379].

[7] M. Burkardt, Phys. Rev. D **62** (2000) 071503 [hep-ph/0005108]; hep-ph/0207047.

[8] J. P. Ralston and B. Pire, hep-ph/0110075.

[9] M. Diehl, Eur. Phys. J. C **25** (2002) 223 [hep-ph/0205208].

[10] S. J. Brodsky, M. Diehl, and D. S. Hwang, Nucl. Phys. B **596** (2001) 99 [hep-ph/0009254]; M. Diehl, T. Feldmann, R. Jakob, and P. Kroll, Nucl. Phys. B **596** (2001) 33 [hep-ph/0009255].

[11] K. Goeke, M. V. Polyakov, and M. Vanderhaeghen, Prog. Part. Nucl. Phys. **47** (2001) 401 [hep-ph/0106012].

[12] J. C. Collins, L. Frankfurt and M. Strikman, Phys. Rev. D **56** (1997) 2982 [hep-ph/9611433]; J. C. Collins and A. Freund, Phys. Rev. D **59** (1999) 074009 [hep-ph/9801262].

[13] M. Diehl, T. Gousset, B. Pire, and J. P. Ralston, Phys. Lett. B **411** (1997) 193 [hep-ph/9706344]; A. V. Belitsky, D. Müller, and A. Kirchner, Nucl. Phys. B **629** (2002) 323 [hep-ph/0112108].

[14] HERMES, A. Airapetian et al., Phys. Rev. Lett. **87** (2001) 182001 [hep-ex/0106068]; V. A. Korotkov and W. D. Nowak, Eur. Phys. J. C **23** (2002) 455 [arXiv:hep-ph/0108077].